Received: 19 November 2019 | Revised: 26 December 2019 | Accepted: 8 January 2020

DOI: 10.1002/ppap.201900233

PLASMA PROCESSES AND POLYMERS

FULL PAPER

Phase mixing in GaSb nanocrystals synthesized by nonequilibrium plasma aerotaxy

Necip B. Uner[1] | **Elijah Thimsen**[1,2]

[1]Department of Energy, Environmental and Chemical Engineering, Washington University in Saint Louis, Saint Louis, Missouri

[2]Institute of Materials Science and Engineering, Washington University in Saint Louis, Saint Louis, Missouri

Correspondence
Elijah Thimsen, Department of Energy, Environmental and Chemical Engineering, Washington University in Saint Louis, Saint Louis, MO 63130.
Email: elijah.thimsen@wustl.edu

Funding information
National Science Foundation, Division of Physics, Grant/Award Number: PHY-1702334; Army Research Office, Grant/Award Number: W911NF-18-1-0240

Abstract

III–V semiconductor nanocrystals are an important class of optoelectronic materials. However, the gas-phase synthesis of these materials, especially of the stibnides, has been left relatively unexplored. In this study, we demonstrate the synthesis of free-standing GaSb nanocrystals for the first time, using a novel gas-phase process. We show that when elemental aerosols are used as precursors for Ga and Sb, the elements mix at the nanometer length scale as the aerosols pass through a nonequilibrium plasma reactor. At sufficiently high plasma power, the mixing produces free-standing GaSb nanocrystals, with a small amount of excess Ga segregated at the periphery of the particles. The reaction is initiated by vaporization of elemental aerosols in the plasma despite the low-background temperature. Ion bombardment determines the extent of vaporization of Ga and Sb and thereby controls the ensemble stoichiometry and reaction rates.

KEYWORDS

aerotaxy, continuous reactor, gallium antimonide, nonthermal plasma, semiconductor nanocrystals

1 | INTRODUCTION

GaSb is a member of the III–V semiconductor family with a direct band gap of 0.73 eV and high hole mobility.[1] The material is promising in many applications, for example, detectors in the short-wave infrared,[2] broadband absorbers in solar and thermophotovoltaic cells,[3] and p-type field-effect and single-hole transistors.[4] The large exciton Bohr radius of GaSb is intriguing as it allows the manufacturing of quantum-confined materials with relative ease. Nanomaterials comprised of GaSb have been investigated, with emphasis placed on the synthesis and characterization of nanowires.[5] Beyond nanowires, spheroidal nanocrystals (NCs) of GaSb are interesting as they can provide beneficial features, especially when used in a free-standing form in charge-based memory devices,[6] or alternatively, when deposited as porous films to make materials with new photonic properties.[7] Studies on the growth of unsupported GaSb NCs, however, have been scarce when compared with the nanowire literature.

Previous studies on the synthesis of unsupported GaSb NCs employed liquid phase methods.[8] There are currently no reports on the gas-phase synthesis of free-standing GaSb NCs. Reported liquid phase GaSb synthesis methods involve procedures that often require more than a day of time to complete, and the GaSb NCs produced by these methods were found to be either heavily agglomerated or impure due to the residual precursor. A gas-phase approach for synthesizing GaSb NCs could provide a chemically pure product, and continuous operation with high yield and decreased cost when compared with liquid phase methods. However, there is a gap in knowledge of how to synthesize free-standing spheroidal GaSb NCs by a gas-phase route.

The process employed in this study is an extension of the recently introduced method termed nonequilibrium plasma aerotaxy (NPA). NPA is a modification of thermal aerotaxy developed by Deppert and Samuelson.[9] In thermal aerotaxy, an aerosol of a constituting element of the desired semiconductor is generated from bulk metals

by evaporation–condensation. Aerosol generation is followed by selecting a specific particle size by differential mobility analysis. Subsequently, the size-selected aerosol is combined with the corresponding vapor precursors of the other elements in the semiconductor and sent into a tube furnace wherein the chemical reaction occurs. In NPA, aerosol precursors are used, similar to thermal aerotaxy. However, no size selection is employed. The entire precursor aerosol is utilized, thereby increasing throughput by several orders of magnitude. Furthermore, the furnace of thermal aerotaxy is replaced by a nonequilibrium plasma. Unipolar negative charging in the nonequilibrium plasma suppresses coagulation due to repulsive Coulombic forces between the particles, and allows the synthesis of free-standing NCs,[10] even at high aerosol concentrations. By using elemental aerosols of Ga, In, and N_2 as the precursors, NPA has been shown to be capable of producing free-standing GaN and InN NCs with tunable size and photonic properties.[11]

In this study, we employ elemental aerosol precursors of high concentration to synthesize GaSb by NPA. Thus, the capabilities of NPA are extended to the synthesis of stibnides, and furthermore, the use of multiple aerosol precursors is demonstrated.

2 | EXPERIMENTAL SECTION

2.1 | Aerosol sources and the aerotaxy setup

Aerosols of Sb and Ga were generated by evaporation–condensation (Figure 1a). The Sb aerosol was generated in a tube furnace. Sb pieces (99.999%; Bayville Chemicals, Deer Park, NY) of approximately 27 g were placed in an alumina boat (Coors Z561738; MilliporeSigma, Darmstadt, Germany), and the boat was inserted into a tube furnace (CM Furnaces Inc., Bloomfield, NJ). To collect the Sb vapor produced, the furnace was swept with 500 standard cubic centimeters per minute (SCCM) ultrahigh purity argon (UHP 5.0; Praxair, Danbury, CT) which was further purified through an alumina-supported copper oxide oxygen scrubber (6300-4SS; Cee Kay, St. Louis, MO). Cooling of the argon-vapor mixture led to rapid formation of the Sb aerosol. The mass output of the furnace was proportional to the vapor pressure of Sb (Figure S1a). When operated at 853 K, the furnace had an Sb aerosol output of 2.30 ± 0.16 mg/min. After a 10 min period of equilibration at the temperature setpoint, which produced a smooth Sb surface in the boat, it was found that the mass output was reproducible (Figure S1b). Although it was previously reported that the furnace aerosol generator is a stable generator,[12] at the high aerosol throughputs used in this study, it was observed that the Sb aerosol mass flow rate drifted with time (Figure S1b). Therefore, all synthesis experiments were conducted within a time window of 12 min, which was the period during which the furnace generator was approximately stable. The furnace generator had a very low mass yield, approximately 1% as most of the Sb aerosol was lost to the walls at the exit of the furnace due to thermophoresis.

The generation of Ga aerosol was accomplished with a hot filament evaporator. Operation of the hot filament evaporator is similar to a hot wire aerosol generator,[13] but unlike the hot wire generator, the hot filament evaporator can produce aerosols from molten metals. Details of the evaporator have been reported previously.[11] Similar to the furnace generator, the evaporator was swept with 500 SCCM Ar. The evaporator was tuned to produce 0.6 mg/min Ga aerosol, and it had steady output over the course of an hour.[11a] The mass yield of the evaporator was an order of magnitude higher than that of the furnace.

Downstream of the evaporation–condensation generators, the precursor aerosol streams were combined at a T-junction. At the exit of the T-junction, Ga and Sb aerosols had mass concentrations of approximately 4.4 and 21 mg/m^3 respectively, and the total number concentration exceeded 10^{15} m^{-3} (see the Supporting Information Data for calculations). The T-junction was followed by a tubular, flow-through, capacitively coupled plasma reactor powered by 13.56 MHz radiofrequency (RF) power (Figure 1b).[14] The plasma reactor is essentially the same as the reactors used in the NPA of GaN and InN.[11] RF power was coupled to a stainless steel ring placed outside the fused silica tube, which acted as the plasma reactor. The tube had 19 mm outer diameter (OD) and 16 mm inner diameter (ID). The steel flange downstream the fused silica tube was grounded. The

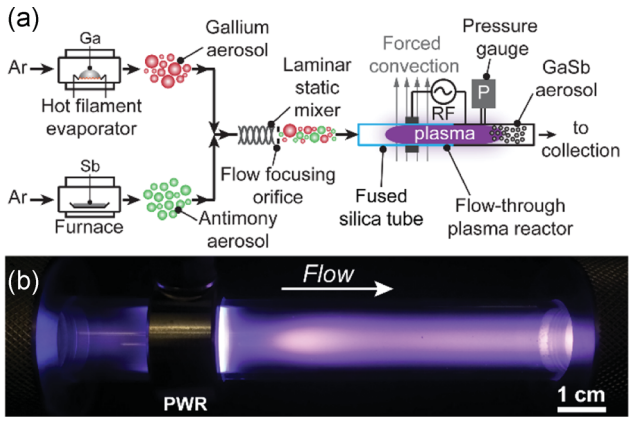

FIGURE 1 (a) Schematic of the nonequilibrium plasma aerotaxy setup for GaSb synthesis. (b) Photograph of the flow-through Ar plasma at 6 Torr and 80 W power. RF, radiofrequency. PWR, powered electrode

pressure in the reactor, and the aerosol generators, was maintained at 6 Torr. Total flow rate through the plasma was 1,000 SCCM, and residence time was approximately 20 ms. The reactor was cooled by two fans.

2.2 | Characterization of the product and the plasma

At a distance of 40 cm downstream of the plasma reactor, particles were collected on stainless steel mesh filters and they were sampled on suspended transmission electron microscopy (TEM) grids for subsequent characterization. Filters were weighed to assess the aerosol mass flow rates. The precursor aerosols were characterized by collecting particles while the plasma was turned off. Images acquired using TEM (JEM-2000 FX; JEOL, Tokyo, Japan) were processed to obtain the primary particle size distributions of the collected aerosols. During image processing, which was done by using ImageJ software, ovals were fitted at the periphery of the particles and the diameter of the area-equivalent circle was taken as particle size. A minimum of 150 particles were counted for each sample. TEM was also used to do elemental analysis by energy-dispersive X-ray spectroscopy (EDXS; Thermo Noran, Waltham, MA), and a higher resolution field-emission microscope (JEM-2100F; JEOL) was used to do EDXS mapping (XFlash 6T; Bruker, Billerica, MA) in scanning mode. The powder collected on filters was subjected to X-ray diffraction (XRD; D8 Advance; Bruker) and qualitative elemental analysis by X-ray fluorescence (XRF; Midex MID01; Spectro, Germany).

The plasma emission was monitored by a modular spectrometer (USB2000+XR1-ES; Ocean Optics, Dunedin, FL) calibrated for relative irradiance. The measurement of the background gas temperature was performed by using a fiber optic temperature probe (OptoTemp 2000; Micromaterials Inc., Tampa, FL).[11a,15] The temperature probe was inserted 1.5 cm downstream of the powered electrode. An RF-compensated double Langmuir probe (Impedans Ltd., Dublin, Ireland) was used to measure the electron temperature and ion density in the absence of aerosols.[16] Platinum tips of 5.8 mm length and 0.37 mm diameter were employed, and the Langmuir probe was inserted through a port 15 cm downstream of the powered electrode. The method of analyzing the I–V curves was outlined in a previous publication.[11a]

3 | RESULTS AND DISCUSSION

When the plasma was off, it was obvious from the deposition patterns on filters that the aerosols did not mix radially throughout the reactor volume (Figure 2a–c). This result is expected because the diffusion path length of the precursor particles is on the order of a millimeter, whereas the diameter of the tubular path between the T-junction and the filter was 16 mm. Therefore, to mix aerosols before they entered the reactor, a laminar static mixer (FMX8481s; Omega Engineering, Norwalk, CT) was installed between the T-junction and the plasma reactor (Figure 2f,g). The mixer provided radial mixing, albeit rather limited, as observed from the swirls of gray (Ga) and black (Sb) on the filter (Figure 2d). Interestingly, a visibly uniform and black deposit was obtained when the mixer was installed and when the plasma was turned on at a power of 80 W (Figure 2e). Scans of X-ray fluorescence across the width of the filters revealed that elements had mixed along the radial dimension when the plasma was on, but not when the plasma was off (Figure 2h,i).

TEM showed that the black uniform powder in Figure 2e was GaSb. The Ga aerosol used for making GaSb was found to be highly polydisperse (Figure 3a), whereas the Sb aerosol was comprised of particles of similar sizes. In spite of their large number concentrations, both precursor aerosols were found to be mostly unagglomerated (Figure S2). The major reason for the absence of agglomerates is the short residence time spent by the precursor aerosols between their production and collection, which is an order of magnitude smaller than the characteristic time of aggregation (Supporting Information Data). With the plasma on during the NPA process, the precursor aerosols appeared to vanish. From those precursor aerosols, GaSb NCs were synthesized (Figure 3c). At 80 W plasma power, the GaSb NCs had a mean diameter of approximately 21 nm, which is between the mean diameters of the precursor aerosols. In addition, the size distribution of GaSb was found to be significantly narrower than those of the precursor aerosols (Figure 3d). The number concentration of the GaSb aerosol was on the order of $10^{14}\ m^{-3}$ (Supporting Information Data). Similar to the source aerosols, the GaSb aerosol was found to be mostly unagglomerated, however, some bridging between the particles was visible (Figure S3). Unlike the precursor aerosols, selective area electron diffraction (SAED) indicated that GaSb particles were crystalline. XRD further proved the crystallinity of the GaSb particles (Figure 3e). No peak corresponding to metallic Sb was visible, however, a broad feature that could be related to metallic Ga was present. A crystallite size of 19 nm was estimated using the Scherrer equation, which is similar to the mean of the size distribution measured using TEM, indicating that GaSb particles were mostly comprised of single crystals.

The formation of GaSb NCs was promoted by the vaporization of precursor aerosols in the plasma. Optical emission spectroscopy indicated the presence of excited

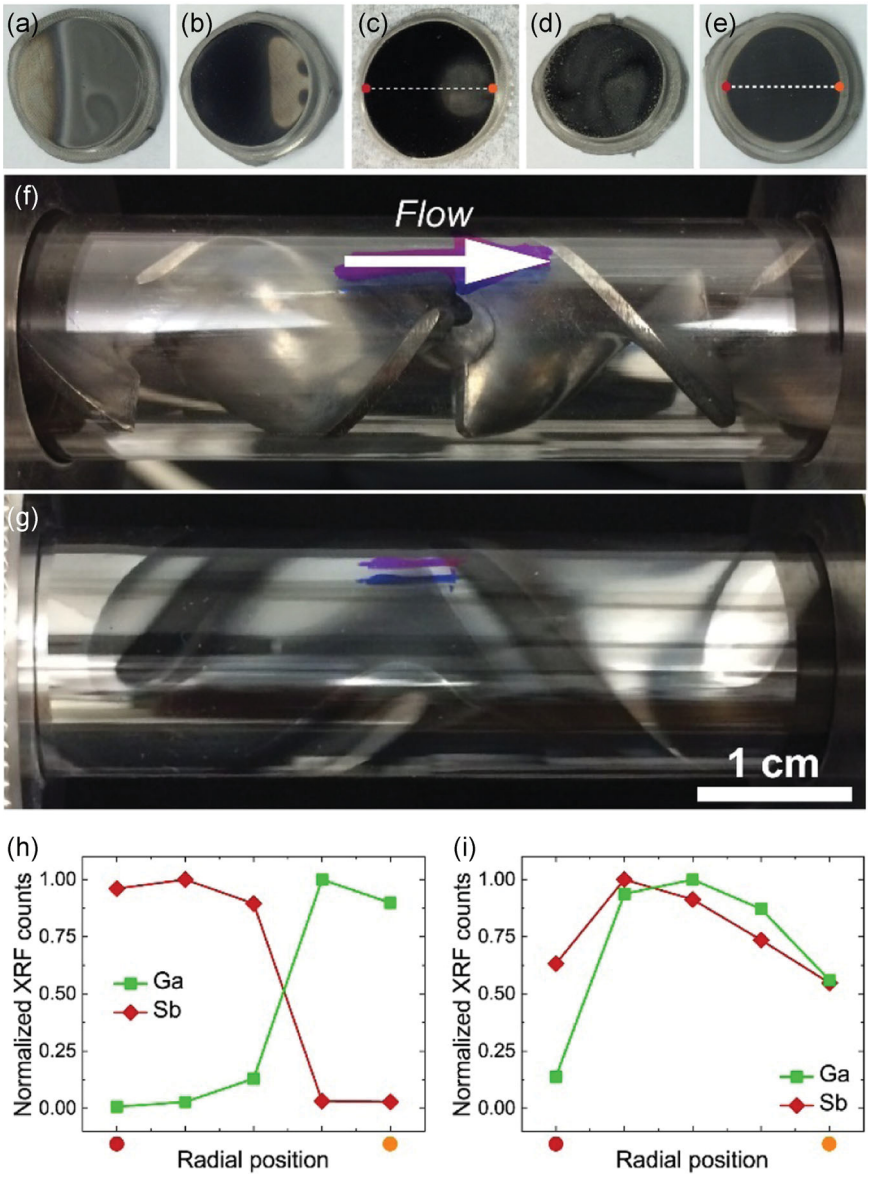

FIGURE 2 (a–e) Filters with particle deposits: (a) Ga, (b) Sb, (c) Ga and Sb without the mixer installed, (d) Ga and Sb particle deposits with the mixer installed, and (e) Ga and Sb deposits with the mixer installed and with the plasma on at 80 W. Helical laminar static mixer, (f) before use, and (g) after use. Shiny gray deposit is Ga and the black deposit is Sb. X-ray fluorescence scans on filters with particle deposits: (h) radial scan on the filter given in (c) along the white dashed line of 16 mm width, plasma was off, and (i) radial scan on the filter given in (e), plasma was on

metal vapors in the plasma at all powers used between 5 and 110 W.[17] Plasma photoemission was collected in an axially integrated manner, as shown in Figure 4a. Figure 4b,c shows the emission spectrum at 80 W when either one of the precursor aerosols was sent into the plasma. The emission spectrum when both Ga and Sb were sent into the plasma is presented in Figure 4d. Emission lines in the ultraviolet, corresponding to Ga I at 403.3 nm ($4s^2 5s \rightarrow 3d^{10} 4s^2 4p$) and Sb I at 326.8 nm ($5p^2(^3P)6s \rightarrow 5p^3$), were clearly visible, despite the low gas temperature, which was <400 K (Figure S4).

Experiments were done to assess the vaporization of either Ga or Sb without the other precursor present. Actinometry was performed as a function of plasma power to estimate the relative vapor amount from the emission spectra (Figure 4b–d insets).[18] The intensity ratio I_{MI}/I_{ArI}, where I_{MI} is the emission from excited metal vapor atoms and I_{ArI} is emission from neutral Ar at 750.4 nm ($3s^2 3p^5(^2P°_{1/2})4p \rightarrow 3s^2 3p^5(^2P°_{1/2})4s$) provides an estimate of the relative vapor content in the plasma.[18] As plasma power was increased, the I_{GaI}/I_{ArI} ratio increased (Figure 4b inset). Qualitatively, the corresponding increase in Ga vapor content can be explained by more intense ion bombardment experienced by the particles at higher applied powers. In the plasma, the ion bombardment rate at the particle surface is typically proportional to ion density, which increases with applied power.[15] Increasing ion bombardment rate can lead to higher particle temperatures,[15,19] and/or higher vaporization rates.[20] In contrast to the I_{GaI}/I_{ArI} ratio, the I_{SbI}/I_{ArI} ratio decreased when power was increased (Figure 4c inset). Although the Ga vapor is monoatomic, Sb primarily forms tetramers in the vapor phase.[21] The expectation is that the dissociation of Sb_4

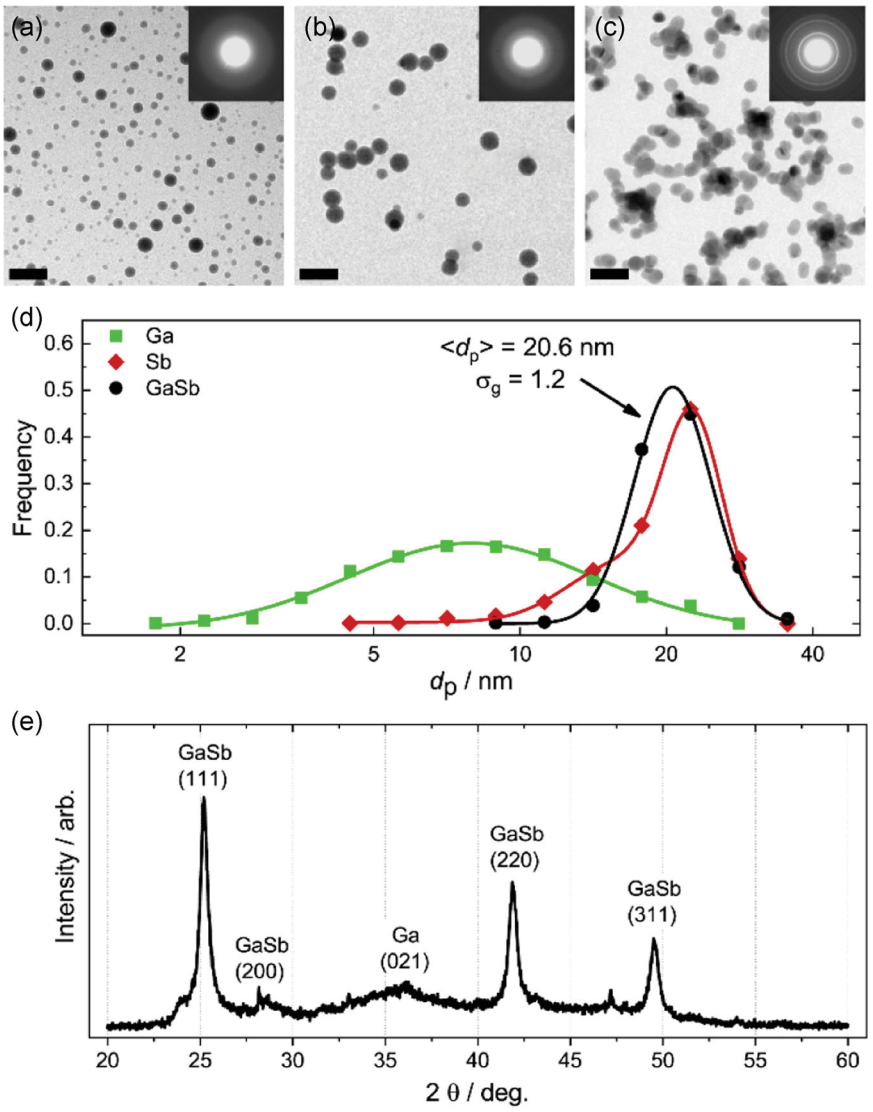

FIGURE 3 Characterization of precursor nanoparticles and GaSb nanocrystals. (a–c) Transmission electron microscopy images. (a) Ga nanoparticles, (b) Sb nanoparticles, (c) GaSb nanocrystals. GaSb nanocrystals were produced at 80 W. Insets are selective area electron diffraction patterns. Scale bars are 50 nm in width. (d) Size distributions of collected Ga, Sb, and GaSb particles. $<d_p>$ is mean diameter, and σ_g is the geometric standard deviation. Size distributions were corrected for sampling bias.[11a] (e) X-ray diffraction pattern of GaSb nanocrystals produced at 80 W

molecules upon increasing power would result in more atomic Sb vapor, thus a more intense Sb I emission. In contrast, the decreasing trend in I_{SbI}/I_{Ar} was likely a manifestation of Sb vapor loss to the reactor walls. Loss of the vapor was visually observed through the rapid formation of a shiny metallic film on the walls of the fused silica tube. The film on the wall was mostly comprised of Sb, and it formed primarily a few centimeters downstream of the powered electrode. The deposition pattern of vapor on the walls is due to the spatial profile of ion density in tubular flow-through plasma reactors, which was previously shown to have a maximum in the vicinity of the powered electrode.[15] A film was deposited on the reactor wall under all conditions investigated. Furthermore, mass yields of both aerosols, especially the yield of antimony, decreased with increasing power.

When both precursor aerosols were sent into the plasma during GaSb synthesis, emission lines from both Ga and Sb were observed (Figure 4d). The presence of these emission lines indicates that both aerosols were vaporized in the plasma. However, under these conditions, Sb vapor is expected to condense on the less volatile Ga particles. At the same time, the presence of both vapors enhances the species exchange between the remaining clusters, which is likely the major cause of mixing of the elements in the radial direction within the reactor volume, as demonstrated in Figures 2e and 2i. When the power was increased, the relative abundance of the Ga vapor increased with respect to the Sb vapor (Figure 4d inset). Although the relative increase in Ga I emission with increasing power could be caused by resonant energy transfer from excited Sb species to Ga vapor, the apparent loss in Sb species at high powers suggests that Ga vapor was increasingly present in the plasma at high powers. A larger amount of Ga vapor in the plasma is expected to cause the Ga content of the product to increase.

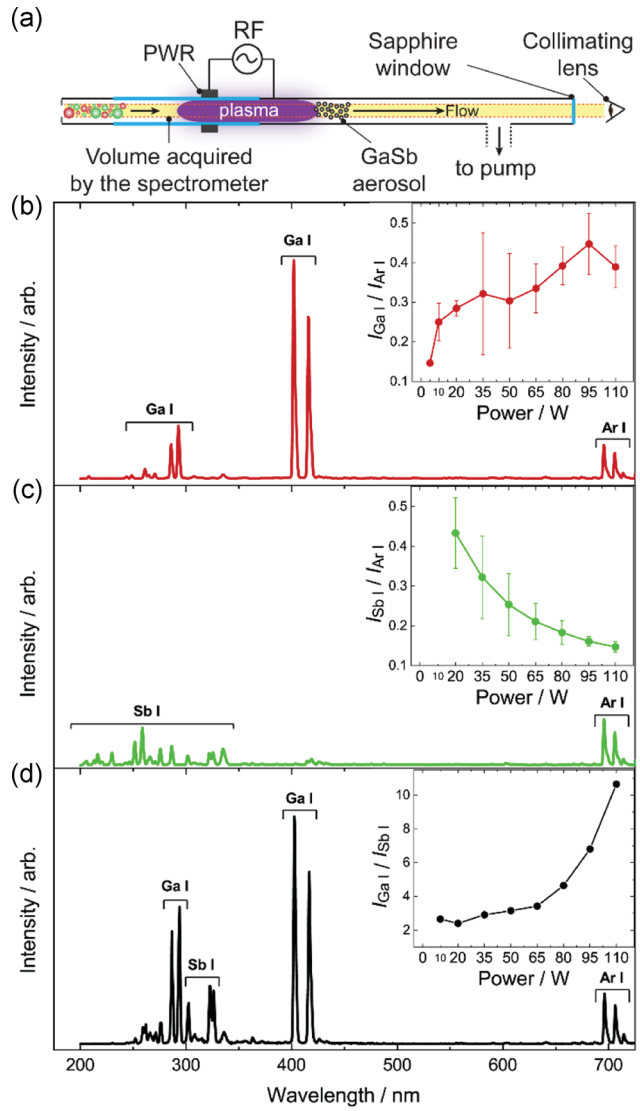

FIGURE 4 Optical emission spectroscopy. (a) Experimental schematic. (b–d) Emission spectra with (b) only Ga aerosol present, (c) only Sb aerosol present, (d) both Ga and Sb aerosols present in the plasma. Insets depict the change in intensity ratios of the indicated lines as a function of plasma power. RF, radiofrequency

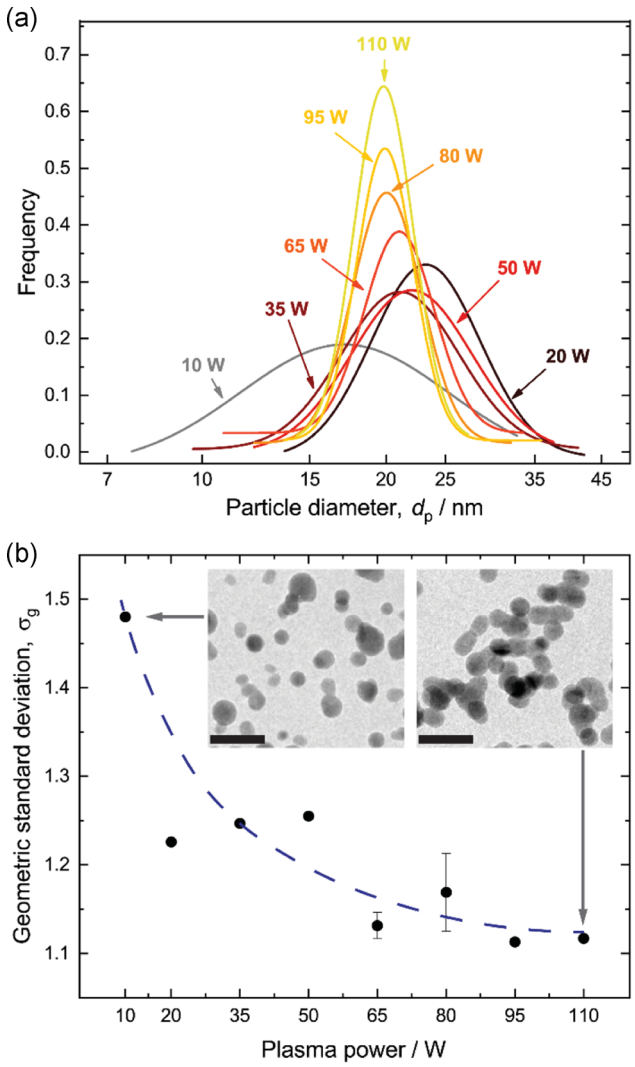

FIGURE 5 Particle size distributions as a function of plasma power. (a) Lognormal fits to size distributions obtained from transmission electron microscopy (TEM). Size distributions were corrected for sampling bias.[11a] (b) Geometric standard deviation of lognormal fits to size distributions given in (a). The dashed line is a guide to the eye. Insets show TEM images of 10 and 110 W samples. Scale bars are 50 nm in width

Over the range of plasma power shown in the inset of Figure 4d, the size distribution of the product aerosol evolved in a distinct manner (Figure 5a). At very low powers, the product aerosol had a broad size distribution, similar to the Ga precursor aerosol, but the mean size was slightly larger. Increasing power first resulted in growth, however, powers >20 W led to a gradual decrease in size. At 80 W, particle size was approximately 20 nm and a further increase in power did not change the size. Interestingly, the widths of the size distributions decreased as power increased and σ_g approached 1.1 (Figure 5b). A possible mechanism for the trends in size and width of the distributions can be given as follows. At low powers, the Sb aerosol preferentially vaporizes, as can be inferred from emission measurements given in Figure 4. This vapor partially condenses on the Ga aerosol, which leads to an aerosol similar to that of Ga precursor aerosol in terms of the width of size distribution, but particles are not as spherical as in the Ga precursor aerosol (Figure 5b inset and Figure 3a). Increasing power initially leads to growth, which might have been caused by a larger amount of Sb vapor scavenged. The slight decrease in size at higher powers and the associated narrowing of the size distribution is expected to occur when all aerosols within the plasma start to vaporize significantly. As power was further increased, an equilibrium size was reached due to the likely decrease in electron temperature in the presence of

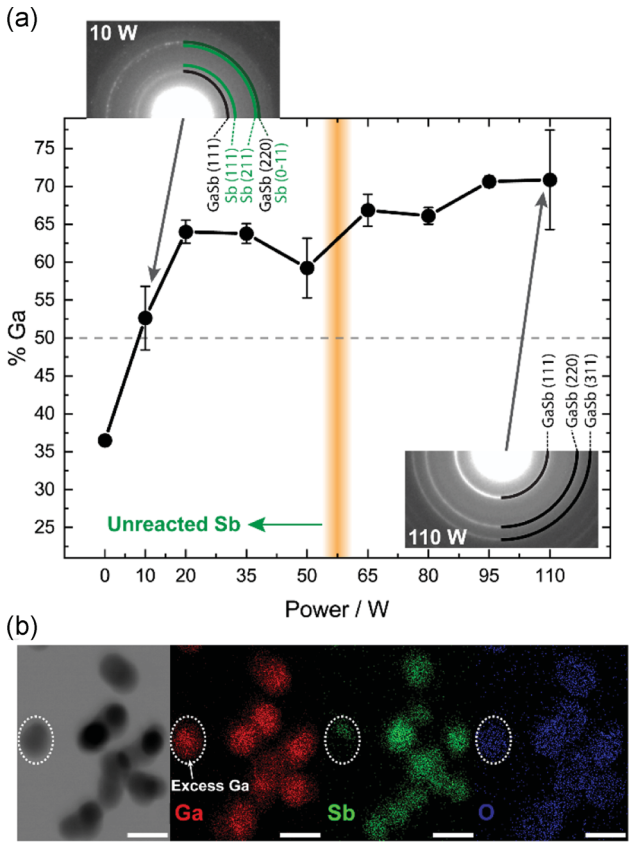

FIGURE 6 (a) Stoichiometry of GaSb nanocrystals measured by energy-dispersive X-ray spectroscopy (EDXS) as a function of plasma power. Insets are selective area electron diffraction (SAED) patterns. Green circles on the SAED images correspond to metallic Sb, and black circles correspond to GaSb. (b) Bright-field image of GaSb NCs synthesized at 80 W and corresponding EDXS maps of constituting elements. Scale bar corresponds to 20 nm

concentrated metallic vapors,[22] which lowered the particle charge and associated ion bombardment. At this stage, condensation–vaporization in the plasma was balanced, and such aerosol dynamics are known to be capable of narrowing the size distribution.[20] Above the 80 W threshold, the widths of the size distributions further decreased at constant mean size. The uniformity of particle size across the whole powder was verified by scraping the powder off the filter, and imaging it under a scanning electron microscope (Figure S5). It is important to note that at powers >80 W, the mass yields were lower. The decrease in mass yield was visible on the filters, as the spot size of black GaSb powder became smaller. At 80 W and higher power, the particles were oblong (Figure 5b inset and Figure S3), which could be due to the formation of a new crystalline phase, that is, GaSb.

Measurements of stoichiometry by EDXS during TEM demonstrated that Ga percentage in the material increased when power was increased, in a trend similar to the Ga vapor in the plasma (Figure 6a). Even when the inlet molar composition was Sb-rich, near 1:1 ensemble stoichiometry was obtained in the product at a very low plasma power of 10 W. However, SAED patterns indicated the presence of metallic Sb at low powers (Figure 6a inset). In other words, the product contained particles with a segregated metallic Sb phase. Even though the change in ensemble stoichiometry with power was small above 20 W, increasing the power beyond 65 W produced mostly oblong particles, and SAED on these particles indicated the presence of GaSb only. At 80 W, we measured an ion density of $1.98 \pm 0.04 \times 10^{18}\ m^{-3}$ and an electron temperature of 1.79 ± 0.04 eV in the absence of aerosols by using the double Langmuir probe. These values are in close agreement with previous measurements done at similar conditions in similar reactors.[11a,15] Crystallization of GaSb thin films requires growth temperatures between 750 and 900 K.[23] Particles can easily reach such temperatures for the plasma parameters measured at higher powers in our reactor.[15] Thus, as power was increased, ion density increased, and consequently, particle temperatures were elevated due to higher ion bombardment rates which lead to crystallization. In other words, above a power threshold, in our case approximately 65 W, particles reach the temperatures necessary for the growth of crystalline GaSb, thereby causing metallic Sb to react with Ga. However, at high powers, NCs had excess Ga, which was not easily visible in SAED due to its amorphous atomic structure.

By EDXS mapping during scanning TEM, it was found that excess Ga was segregated, and was usually located as an outer shell on the particles (Figure 6b). This preferential location of Ga at the surface could be a result of Ga being in the liquid phase due to melting point depression as a consequence of small particle size.[24] It is important to note that GaSb nanoparticles were previously found to be sensitive to phase segregation caused by electron beam damage,[25] likely due to the low enthalpy of formation of GaSb (−45.9 kJ/mol),[26] therefore some of the local deviations from 1:1 stoichiometry might have formed in situ during TEM. Nevertheless, EDXS mapping indicated that there was good local mixing of Ga and Sb in the NCs. The GaSb NCs had a thin native oxide, likely caused by air exposure during handling.

Adjustment of the GaSb stoichiometry in the NPA process can be accomplished by several means. The most convenient approach is to increase the initial molar ratio of Sb to Ga. However, preliminary experiments indicated that whenever the mass throughput was increased, plasma power must also be increased to obtain a well-mixed product. If the plasma power was held constant as the mass throughput was increased, then significant amounts of unreacted Sb and Ga were observed in the product (Figure S6). In other words,

ensemble stoichiometry can be tuned by adjusting inlet mass concentrations of precursor aerosols, however, providing the optimal ion bombardment conditions for complete reaction is also dependent on the aerosol concentration in the plasma. The result suggests that ion and electron bombardment, and associated properties, such as particle charge and temperature, can be strongly dependent on the aerosol concentration in synthesis plasmas, perhaps due to a decrease in electron temperature in the presence of metallic vapors and aerosols of high concentration. Another method to adjust the GaSb stoichiometry could be acid etching during post-processing. HCl treatment could remove some of the excess Ga at the periphery of the GaSb nanocrystals. An alternative and interesting approach would be conducting the GaSb synthesis in the presence of a gaseous pnictogen, which might allow the consumption of excess Ga and at the same time yield ternary semiconductor nanocrystals with different morphologies.

Although the exact mechanism for NPA of III–V semiconductors is not entirely clear, the results discussed in the preceding paragraphs present a qualitative overview of the mechanism. It can be summarized as follows. The precursor aerosols vaporize near the powered electrode, where the ion density is higher. The Sb aerosol vaporizes much more than the Ga aerosol, and downstream of the vaporization zone, some of the Sb vapor condenses on the Ga aerosol that did not vaporize. This vapor transport mechanism is a unique feature of NPA. Therefore, it is this mechanism that differentiates the plasma from a thermal reactor, such as a furnace. Unlike a furnace, in NPA, the elements are mixed in a largely nonthermal background. Furthermore, the gradients in the background temperature in the plasma are less severe than those of a furnace. As a result, thermophoretic losses in a plasma reactor are expected to be much less than in a furnace reactor. This issue is apparent in the present work as a very low yield of Sb aerosol from the furnace aerosol generator was employed in this study. Upon the completion of vapor transport, the mixed aerosol continues to travel within the plasma. In this part of the plasma with a lower ion density, rapid solid-state reaction between Ga and Sb occurs to yield crystalline GaSb if the requisite ion bombardment rates are provided. In our experiments, this threshold was demonstrated by increasing power, and consequently, by increasing ion density. However, some excess Ga was found to be segregated from the GaSb phase, especially at the periphery of the particles. The excess Ga did not increase or decrease substantially with increasing power, but the overall mass yield decreased. In situ diagnostics on plasma synthesis would help to elucidate the dynamics of growth in NPA, especially when two precursor aerosols with different physiochemical properties, such as Ga and Sb, are used.

4 | CONCLUSION

In conclusion, a new process was presented for synthesizing free-standing GaSb nanocrystals. The method, termed NPA, was extended to allow the synthesis of GaSb nanocrystals from elemental aerosol precursors. These precursor aerosols were found to vaporize in the nonequilibrium plasma. The presence of the elemental vapor, especially that of Sb, led to a redistribution of Sb across the whole aerosol with little to no aggregation. When the plasma power was sufficiently high, Ga and Sb elements reacted and mixed rapidly at the nanometer scale, thereby forming GaSb nanocrystals with narrow size distributions. It was found that the product was typically rich in the less volatile element, in this case, Ga. The process may allow the synthesis of binary or ternary semiconductor nanocrystals that are free from organic contaminants.

ACKNOWLEDGMENTS

The authors acknowledge financial support from the Army Research Office MURI grant W911NF-18-1-0240 and from the National Science Foundation grant PHY-1702334. This study was performed in part at the Institute of Materials Science and Engineering at Washington University in Saint Louis.

ORCID

Necip B. Uner http://orcid.org/0000-0002-5719-6417
Elijah Thimsen http://orcid.org/0000-0002-7619-0926

REFERENCES

[1] P. S. Dutta, H. L. Bhat, V. Kumar, *J. Appl. Phys.* **1997**, *81*, 5821.
[2] S. Bandyopadhyay, J. Anderson, *Appl. Phys. Lett.* **2013**, *102*, 103108.
[3] (a) N. J. Ekins-Daukes *Solar Cell Materials: Developing Technologies* (Eds: G. J. Conibeer, A. Willoughby), John Wiley & Sons, Chichester, West Sussex, UK **2014**; (b) V. S. Mangu, E. J. Renteria, S. J. Addamane, A. Mansoori, A. Armendáriz, C. F. Deneke, S. O. Ferreira, M. Zamiri, G. Balakrishnan, F. Cavallo, *Appl. Phys. Lett.* **2018**, *113*, 123502; (c) C. W. Hitchcock, R. J. Gutmann, J. M. Borrego, I. B. Bhat, G. W. Charache, *IEEE Trans. Electron Devices* **1999**, *46*, 2154.
[4] (a) W. Xu, A. Chin, L. Ye, C. Z. Ning, H. Yu, *J. Appl. Phys.* **2012**, *111*, 104515; (b) B. Ganjipour, H. A. Nilsson, B. Mattias Borg, L.-E. Wernersson, L. Samuelson, H. Q. Xu, C. Thelander, *Appl. Phys. Lett.* **2011**, *99*, 262104.
[5] (a) B. M. Borg, L.-E. Wernersson, *Nanotechnology* **2013**, *24*, 202001; (b) E. Barrigón, M. Heurlin, Z. Bi, B. Monemar, L. Samuelson, *Chem. Rev.* **2019**, *119*, 9170.
[6] M. Califano, P. Rodosthenous, *ACS Appl. Mater. Interfaces* **2019**, *11*, 640.

[7] C. Yan, X. Li, K. Zhou, A. Pan, P. Werner, S. L. Mensah, A. T. Vogel, V. Schmidt, *Nano Lett.* **2012**, *12*, 1799.
[8] (a) S. Schulz, L. Martinez, J. L. Ross, *Adv. Mater. Opt. Electron.* **1996**, *6*, 185; (b) R. A. Baldwin, E. E. Foos, R. L. Wells, *Mater. Res. Bull.* **1997**, *32*, 159; (c) S. Schulz, W. Assenmacher, *Mater. Res. Bull.* **1999**, *34*, 2053; (d) H.-L. Li, Y.-C. Zhu, O. Palchik, Y. Koltypin, A. Gedanken, V. Palchik, M. Slifkin, A. Weiss, *Inorg. Chem.* **2002**, *41*, 637.
[9] K. Deppert, L. Samuelson, *Appl. Phys. Lett.* **1996**, *68*, 1409.
[10] U. R. Kortshagen, R. M. Sankaran, R. N. Pereira, S. L. Girshick, J. J. Wu, E. S. Aydil, *Chem. Rev.* **2016**, *116*, 11061.
[11] (a) N. B. Uner, E. Thimsen, *J. Phys. Appl. Phys.* **2019**, *53*, 095201; (b) N. B. Uner, D. M. Niedzwiedzki, E. Thimsen, *J. Phys. Chem. C* **2019**, *123*, 30613.
[12] H. G. Scheibel, J. Porstendörfer, *J. Aerosol Sci.* **1983**, *14*, 113.
[13] (a) A. M. Boies, P. Lei, S. Calder, W. G. Shin, S. L. Girshick, *Aerosol Sci. Technol.* **2011**, *45*, 654; (b)A. Izadi, R. J. Anthony, *Plasma. Process. Polym.* **2019**, *16*, e1800212.
[14] L. Mangolini, E. Thimsen, U. Kortshagen, *Nano Lett.* **2005**, *5*, 655.
[15] N. B. Uner, E. Thimsen, *Plasma Sources Sci. Technol.* **2018**, *27*, 074005.
[16] E. O. Johnson, L. Malter, *Phys. Rev.* **1950**, *80*, 58.
[17] A. Kramida, Y. Ralchenko, J. Reader, NIST ASD Team, "NIST Atomic Spectra Database (ver. 5.3)," http://physics.nist.gov/asd, 2015. Accessed October 13, 2019.
[18] J. W. Coburn, M. Chen, *J. Appl. Phys.* **1980**, *51*, 3134.
[19] (a) L. Mangolini, U. Kortshagen, *Phys. Rev. E* **2009**, *79*, 026405; (b) H. R. Maurer, H. Kersten, *J. Phys. Appl. Phys.* **2011**, *44*, 174029.
[20] N. B. Uner, E. Thimsen, *J. Phys. Chem. C* **2017**, *121*, 12936.
[21] G. M. Rosenblatt, C. E. Birchenall, *J. Chem. Phys.* **1961**, *35*, 788.
[22] A. Von Engel, *Ionized Gases*, AIP Press, Woodbury, NY **1994**.
[23] (a) S. K. Haywood, N. J. Mason, P. J. Walker, *J. Cryst. Growth* **1988**, *93*, 56; (b) C. A. Wang, S. Salim, K. F. Jensen, A. C. Jones, *J. Cryst. Growth* **1997**, *170*, 55; (c) K. Akahane, N. Yamamoto, S. Gozu, N. Ohtani, *J. Cryst. Growth* **2004**, *264*, 21.
[24] A. N. Goldstein, C. M. Echer, A. P. Alivisatos, *Science* **1992**, *256*, 1425.
[25] (a) H. Yasuda, H. Mori, J. G. Lee, *Phys. Rev. B* **2004**, *70*, 214105; (b)H. Yasuda, A. Tanaka, H. Usui, H. Mori, J. G. Lee, *Eur. Phys. J. D* **2006**, *37*, 231; (c) H. Yasuda, A. Tanaka, H. Usui, H. Mori, J. G. Lee, *Eur. Phys. J. D* **2007**, *43*, 177.
[26] K. Yamaguchi, Y. Takeda, K. Kameda, K. Itagaki, *Mater. Trans., JIM* **1994**, *35*, 596.

SUPPORTING INFORMATION

Additional supporting information may be found online in the Supporting Information section.

How to cite this article: Uner NB and Thimsen E. Phase mixing in GaSb nanocrystals synthesized by nonequilibrium plasma aerotaxy. *Plasma Process Polym*. 2020;e1900233.
https://doi.org/10.1002/ppap.201900233